Journal of Sound and Vibration 329 (2010) 1062–1080

Contents lists available at ScienceDirect

Journal of Sound and Vibration

journal homepage: www.elsevier.com/locate/jsvi

The wave-based substructuring approach for the efficient description of interface dynamics in substructuring

S. Donders [a,*], B. Pluymers [b], P. Ragnarsson [a], R. Hadjit [a], W. Desmet [b]

[a] LMS International, Interleuvenlaan 68, B-3001 Leuven, Belgium
[b] K.U.Leuven, Department of Mechanical Engineering, Celestijnenlaan 300 B, B-3001 Heverlee, Belgium

ARTICLE INFO

Article history:
Received 6 April 2009
Received in revised form
12 October 2009
Accepted 15 October 2009
Handling Editor: A.V. Metrikine

ABSTRACT

In the vehicle design process, design decisions are more and more based on virtual prototypes. Due to competitive and regulatory pressure, vehicle manufacturers are forced to improve product quality, to reduce time-to-market and to launch an increasing number of design variants on the global market. To speed up the design iteration process, substructuring and component mode synthesis (CMS) methods are commonly used, involving the analysis of substructure models and the synthesis of the substructure analysis results. Substructuring and CMS enable efficient decentralized collaboration across departments and allow to benefit from the availability of parallel computing environments. However, traditional CMS methods become prohibitively inefficient when substructures are coupled along large interfaces, i.e. with a large number of degrees of freedom (DOFs) at the interface between substructures. The reason is that the analysis of substructures involves the calculation of a number of enrichment vectors, one for each interface degree of freedom (DOF). Since large interfaces are common in vehicles (e.g. the continuous line connections to connect the body with the windshield, roof or floor), this interface bottleneck poses a clear limitation in the vehicle noise, vibration and harshness (NVH) design process. Therefore there is a need to describe the interface dynamics more efficiently. This paper presents a wave-based substructuring (WBS) approach, which allows reducing the interface representation between substructures in an assembly by expressing the interface DOFs in terms of a limited set of basis functions (“waves”). As the number of basis functions can be much lower than the number of interface DOFs, this greatly facilitates the substructure analysis procedure and results in faster design predictions. The waves are calculated once from a full nominal assembly analysis, but these nominal waves can be re-used for the assembly of modified components. The WBS approach thus enables efficient structural modification predictions of the global modes, so that efficient vibro-acoustic design modification, optimization and robust design become possible. The results show that wave-based substructuring offers a clear benefit for vehicle design modifications, by improving both the speed of component reduction processes and the efficiency and accuracy of design iteration predictions, as compared to conventional substructuring approaches.

* Corresponding author.
E-mail address: stijn.donders@lmsintl.com (S. Donders).

0022-460X/$ - see front matter © 2009 Elsevier Ltd. All rights reserved.
doi:10.1016/j.jsv.2009.10.022

1. Introduction

Driving factors in modern automotive product development include the steadily increasing customer demands and competitive nature of the market. Automotive design engineers face the challenging and complex problem of meeting ever expanding but often conflicting design criteria and legislations. As time-to-market and development costs must be reduced, physical prototype phases must be shortened, and product decisions must be taken earlier in the design process [1,2]. The additional trend of mass customization forces engineers to design a higher number of variants on a lower number of platforms. To overcome this increasing demand of computer calculation resources, fast assembly predictions become ever more important in the vehicle development process and the design decisions are more and more based on virtual prototypes.

1.1. Different approaches to component mode synthesis

The finite element (FE) method [3,4] has become the most popular deterministic technique to predict the vibro-acoustic performance of mechanical structures. In automotive industry, the method is extensively used for modal analysis and interior acoustics prediction of vehicles [5–7]. With increasing frequency, the model size (and hence the computational costs) must increase to maintain the prediction accuracy. This limits the applicability of the FE method to the low and medium frequency range, even with today's powerful computers [8,9].

To partially overcome this practical limit, extensive work has been performed on substructuring and component mode synthesis (CMS) techniques [10]. By dividing the structure into smaller parts, solving the substructures individually and then recombining the substructure results into a system-level solution, more efficient calculation schemes can be achieved. The degrees of freedom (DOFs) of each substructure are expressed in terms of a limited number of component modes; the component models are then synthesized. A range of CMS methods has been reported in the literature, as overviewed in e.g. [11–14]. All methods make use of the vibration normal modes of the substructures but they differ in the boundary conditions that are applied to the substructures and in the selection of enrichment vectors to these normal modes. Two well-established CMS methods are:

(1) The Craig–Bampton fixed interface approach [10,15], for which the normal modes are computed while the substructure is clamped at the connection interface, and for which the enrichment vectors consist of constraint modes (which are the static deformation shapes of the substructure obtained by successively applying a unit displacement on one interface degree of freedom, while holding the remaining interface DOFs fixed, and repeating this for all interface DOFs).
(2) The approach of MacNeal [16] and Rubin [17] uses the normal modes of the component in free–free conditions, and enrichment vectors that consist of residual flexibility modes (which are the static deformation shapes obtained by successively applying a unit force on one of the interface degrees of freedom, with a zero force on the remaining interface DOFs, and repeating this for all interface DOFs).

1.2. Reduction of the interface representation size

The well-established CMS methods reported in the previous section perform a reduction procedure, in which, in a first phase of the calculation, the component normal modes are calculated (with method-dependent boundary conditions). In a second phase, an additional static vector is then calculated for each interface DOF (namely a constraint mode for Craig–Bampton, and a residual attachment mode for MacNeal and Rubin, respectively). This second calculation step implies that the efficiency of the procedure decreases when the number of interface DOFs increases. In case of a small interface, the extra effort involved in calculating the additional static vectors is rather small. However, for a large interface, this calculation may become prohibitively expensive in terms of CPU time.

To further speed up the synthesis, the interface representation size between components must be reduced. Previous papers have reported on the use of component modes to derive the interface basis functions [18]. Ji et al. [19] have developed a procedure to use component modes to derive interface basis functions that efficiently describe the interface between two substructures. They consider this in a forced response context, with a source substructure and receiver substructure. The source and receiver substructures are described with uncoupled modes. The presented applications are limited to plates and beams, for which the component modes are obtained as an infinite series of orthogonal basis functions that are truncated at a certain number. The interface forces and displacements are decomposed into a set of complete and orthogonal basis functions, and the equilibrium and continuity conditions are subsequently enforced in terms of basis functions. This way, the physical coupling DOFs of the built-up structure are transferred into generalized coupling DOFs. This can potentially give accurate, approximate models using a reduced number of DOFs, however, only in the case that the global interface displacements can indeed be described accurately in terms of component modes. In the extreme case of coupling a very stiff component with a very flexible component, an obvious choice is to derive the interface basis functions from the component modes of the stiff component. This is indeed the application reported in [19], in which a stiff beam is coupled to a flexible plate in a forced response context. The beam acts as the long-wavelength source,

coupled to the short-wavelength plate. It is shown that a limited number of mode shapes of the stiff beam can be used to accurately describe the interface dynamics. This approach is indeed promising for such extreme cases, and has industrial value (e.g. to study the response of a flexible floor structure to the source input from a stiff piece of machinery), but it is not generally applicable. The approach is not suitable to describe the interface of components with similar modal densities (for which the global system dynamics differs substantially from the component dynamics).

Brahmi et al. [20] use the terminology of "junction DOFs" as a synonym for "interface DOFs"; in this paper, both these terms will be used as synonyms. Brahmi et al. present a method to reduce the number of junction DOFs in a component mode synthesis method, based on the use of interface modes. These are obtained from solving the Guyan eigenvalue problem. The junction DOFs are then expressed in terms of these interface modes. A similar approach is used by Tran [11], who first calculates the constraint modes for the global structure, and projects the global stiffness matrix and mass matrix of the structure on the global constraint modes to obtain the reduced stiffness matrix and the reduced mass matrix. A Guyan eigenvalue problem can then be defined and the solution yields a set of interface modes which can be used as enrichment vectors in CMS, instead of the (much) larger set of constraint modes.

Castanier et al. [21] describe a technique for reducing the size of a model generated by a Craig–Bampton method. The method is based on performing an eigenanalysis on the constraint-mode partitions of the mass and stiffness matrices that correspond to the Craig–Bampton constraint modes. This way, the characteristic constraint modes are obtained. These are the characteristic deformation shapes of the interface, which may be truncated in the same way as natural modes of vibration. The method of Castanier et al. does require the calculation of a full Craig–Bampton model, for which the interface description can then be strongly reduced when the characteristic constraint modes are used instead of the constraint modes. The authors mention that the characteristic constraint modes give insight in the physical mechanisms of vibration transmission between substructures. This makes the method especially suited for power flow prediction in complex substructures. The CCM method shares the computational disadvantage of the Craig–Bampton method when a large number of interface DOFs are involved, which is the case amongst others for line and surface connections between components in complex mechanical systems. The presented WBS method alleviates the computational cost for calculating all enrichment vectors, by proposing a way to directly calculate the enrichment vectors of interest, without first having to calculate the entire set, and making a subsequent condensation thereof.

Work has also been performed on different ways to increase the accuracy when studying design modifications [22].

1.3. Wave based substructuring: outline of the paper

In the former, it has been elaborated that reducing the interface description is of great value in CMS to speed up the calculations. Several methods to reduce the interface description have been reported up to now, exploiting either static reduction or component modes to reduce the interface description. Reported methods are, however, limited in terms of accuracy or applicability. That is, an approach that allows reduction of the interface in the entire dynamic frequency range of interest, which takes the dynamics of the assembly model into account, and which is valid also for the assembly of substructures with similar modal density, has not yet been reported. The wave-based substructuring (WBS) approach, for which preliminary results have been reported in [23,24], is presented in this paper as a method that is in line with these requirements. Section 2 gives a detailed overview of the WBS approach. In WBS, a single modal analysis computation of the full assembly model is performed in order to obtain the interface basis functions. The interface displacements of substructures are then described by a limited set of interface basis functions ("waves"). As the required number of basis functions is typically much lower than the number of interface DOFs, faster assembly predictions are obtained as compared to the CMS method of MacNeal [16] and Rubin [17]. Since the waves are calculated from the full assembly model, the interface dynamics are accurately captured, even when coupling components with similar modal density. The waves obtained from a full nominal assembly analysis can be re-used for the assembly of modified components. With modification analysis and optimization in mind, and also for robust design and uncertainty assessment [13,14], a single full computation is not a large burden, as an optimization may consist of numerous iterations involving hundreds of FE runs. The single full run in WBS enables that the interface representation size is reduced, which facilitates the model reduction procedure of components and speeds up the assembly analysis, while the accuracy is maintained. In Section 3, the efficiency and accuracy of WBS (as compared to the conventional MacNeal–Rubin substructuring procedure) are demonstrated on the basis of two application cases, namely a two-plate assembly case and an industrial vehicle BIW case aimed at efficient re-design of the B-pillars. On the basis of the latter case, Section 4 shows that WBS can be used for efficient design modifications in view of reaching global vibro-acoustic performance targets. The paper is concluded in Section 5.

2. Theory of wave-based substructuring

2.1. Matrix equations of substructuring

Consider the general undamped structure S to which no external forces are applied. The FE matrix equation for the assembled system is given by

$$\mathbf{M}\ddot{\mathbf{x}} + \mathbf{K}\mathbf{x} = 0 \tag{1}$$

Let this structure be decomposed into N_s non-overlapping substructures. For each substructure (denoted with superscript $^{(s)}$, with $s=1\ldots N_s$), the DOFs are decomposed into interior DOFs (subscript i) and junction DOFs (subscript j) at the interface. The equation of motion of each substructure can then be written in matrix form as

$$\begin{bmatrix} \mathbf{M}_{ii} & \mathbf{M}_{ij} \\ \mathbf{M}_{ji} & \mathbf{M}_{jj} \end{bmatrix}^{(s)} \begin{Bmatrix} \ddot{\mathbf{x}}_i \\ \ddot{\mathbf{x}}_j \end{Bmatrix}^{(s)} + \begin{bmatrix} \mathbf{K}_{ii} & \mathbf{K}_{ij} \\ \mathbf{K}_{ji} & \mathbf{K}_{jj} \end{bmatrix}^{(s)} \begin{Bmatrix} \mathbf{x}_i \\ \mathbf{x}_j \end{Bmatrix}^{(s)} = \begin{Bmatrix} 0 \\ \mathbf{f}_j \end{Bmatrix}^{(s)} \tag{2}$$

For an example structure consisting of two substructures (a) and (b), this process is visualized in Fig. 1. The junction (or boundary) DOFs are denoted $\mathbf{x}_j^{(a)}$ and $\mathbf{x}_j^{(b)}$, and the interior DOFs are denoted $\mathbf{x}_i^{(a)}$ and $\mathbf{x}_i^{(b)}$, respectively.

To assemble the substructures, equilibrium and continuity conditions must be applied to the reduced matrix equations of the substructures. This may require rigid or elastic connections.

Rigid connection: A rigid connection between two substructures (a) and (b) can be created by applying continuity of the interface displacements and the equilibrium of the interface reactions:

$$\mathbf{x}_j^{(a)} = \mathbf{x}_j^{(b)} \quad \text{and} \quad \mathbf{f}_j^{(a)} + \mathbf{f}_j^{(b)} = 0 \tag{3}$$

Elastic connection: In some cases, the nominal model may have an elastic connection along the interface (e.g. in vehicle assembly, the glue connection between windscreen and body in white (BIW)). The equilibrium and continuity condition in Eq. (4) can then be applied to create an elastic connection between two substructures (a) and (b). Here, the matrices $\mathbf{K}^e$ represent the elastic coupling stiffness matrices between the junction DOFs of the substructures. An alternative formulation can be derived for cases in which more than two substructures are connected along an interface

$$\begin{bmatrix} \mathbf{f}_j^{(a)} \\ \mathbf{f}_j^{(b)} \end{bmatrix} = \begin{bmatrix} \mathbf{K}_{aa}^e & \mathbf{K}_{ab}^e \\ \mathbf{K}_{ba}^e & \mathbf{K}_{bb}^e \end{bmatrix} \begin{bmatrix} \mathbf{x}_j^{(a)} \\ \mathbf{x}_j^{(b)} \end{bmatrix} \tag{4}$$

when the number of junction DOFs is large, the "reduction" step to solve individual substructures may become a bottleneck, since the number of junction DOFs determines the speed and memory requirements of the modal reduction procedure. For the reduction of a substructure in a given frequency range of interest on a given computer system, this means that it may no longer be feasible to perform the reduction procedure when the interface representation size is larger than a certain number of junction DOFs. Moreover, when reduced substructure models are assembled, the size of the assembled system will be dominated by the size of the junction DOFs.

2.2. Matrix equations for wave-based substructuring

2.2.1. A wave-based formulation of the junction DOFs

Consider the substructure (s), which has $n_j^{(s)}$ junction DOFs $\mathbf{x}_j$. To reduce the interface description, a set of $n_w^{(s)}$ basis functions $\mathbf{W}^{(s)}$ can be used to express the junction DOFs $\mathbf{x}_j^{(s)}$ as a linear combination of $\mathbf{W}^{(s)}$:

$$\mathbf{x}_j^{(s)} = \mathbf{W}^{(s)} \cdot \mathbf{p}^{(s)} \tag{5}$$

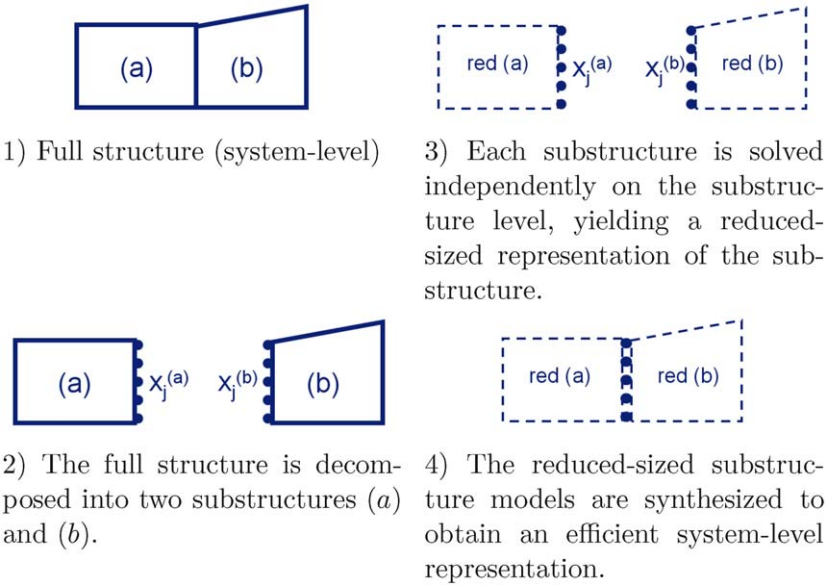

Fig. 1. Domain decomposition and CMS, visualized for an example structure consisting of two substructures (a) and (b), with junction (or boundary) DOFs $\mathbf{x}_j^{(a)}$ and $\mathbf{x}_j^{(b)}$, and interior DOFs $\mathbf{x}_i^{(a)}$ and $\mathbf{x}_i^{(b)}$, respectively.

Substitution of Eq. (5) in Eq. (2) yields the following equation for each substructure (s) (where substructure indices (s) are omitted for convenience):

$$\begin{bmatrix} \mathbf{M}_{ii} & \mathbf{M}_{ij}\mathbf{W} \\ \mathbf{W}^{\mathrm{T}}\mathbf{M}_{ji} & \mathbf{W}^{\mathrm{T}}\mathbf{M}_{jj}\mathbf{W} \end{bmatrix} \begin{Bmatrix} \ddot{\mathbf{x}}_i \\ \ddot{\mathbf{p}} \end{Bmatrix} + \begin{bmatrix} \mathbf{K}_{ii} & \mathbf{K}_{ij}\mathbf{W} \\ \mathbf{W}^{\mathrm{T}}\mathbf{K}_{ji} & \mathbf{W}^{\mathrm{T}}\mathbf{K}_{jj}\mathbf{W} \end{bmatrix} \begin{Bmatrix} \mathbf{x}_i \\ \mathbf{p} \end{Bmatrix} = \begin{Bmatrix} 0 \\ \mathbf{W}^{\mathrm{T}}\mathbf{f}_j \end{Bmatrix} \tag{6}$$

From here on, the basis functions are denoted "waves". Provided that the number of waves $n_w^{(s)}$ is less than the number of junction DOFs $n_j^{(s)}$, this substitution reduces the size of the interface representation.

2.2.2. Wave-based assembly definition

To create an assembly of substructures, equilibrium and continuity must be applied to the reduced matrix equations of the substructures, which now have the form in Eq. (6). Without loss of generality, consider again the visualization example with two substructures (a) and (b) in Fig. 1. Using Eq. (5) for each substructure, the junction DOFs $\mathbf{x}_j^{(a)}$ and $\mathbf{x}_j^{(b)}$ are expressed as a linear combinations of two sets of interface basis functions, by substituting $\mathbf{x}_j^{(a)} = \mathbf{W}^{(a)} \cdot \mathbf{p}^{(a)}$ and $\mathbf{x}_j^{(b)} = \mathbf{W}^{(b)} \cdot \mathbf{p}^{(b)}$, respectively, as shown in Fig. 2.

A connection between the waves $\mathbf{p}^{(a)}$ and $\mathbf{p}^{(b)}$ on each side must now be made. Again, rigid or elastic connections can be defined, with equilibrium and continuity conditions defined in terms of waves.

Rigid connection: A rigid connection between two substructures (a) and (b) can be made when the same waves are used at each side of the connection ($\mathbf{W}^{(a)} = \mathbf{W}^{(b)}$). Continuity of the wave participation factors at each side, and conventional equilibrium of interface forces, then results in a rigid connection:

$$\mathbf{p}^{(a)} = \mathbf{p}^{(b)} \quad \text{and} \quad \mathbf{f}_j^{(a)} + \mathbf{f}_j^{(b)} = 0 \tag{7}$$

Elastic connection: In the elastic equilibrium and continuity condition in Eq. (4), the same substitutions $\mathbf{x}_j^{(a)} = \mathbf{W}^{(a)} \cdot \mathbf{p}^{(a)}$ and $\mathbf{x}_j^{(b)} = \mathbf{W}^{(b)} \cdot \mathbf{p}^{(b)}$ can be made (according to Eq. (5)). After multiplying the first row with $\mathbf{W}^{(a)\mathrm{T}}$ and the second row with $\mathbf{W}^{(b)\mathrm{T}}$, the following elastic equilibrium and continuity condition between waves is obtained:

$$\begin{bmatrix} \mathbf{W}^{(a)\mathrm{T}}\mathbf{f}_j^{(a)} \\ \mathbf{W}^{(b)\mathrm{T}}\mathbf{f}_j^{(b)} \end{bmatrix} = \begin{bmatrix} \mathbf{W}^{(a)\mathrm{T}}\mathbf{K}_{aa}^{e}\mathbf{W}^{(a)} & \mathbf{W}^{(a)\mathrm{T}}\mathbf{K}_{ab}^{e}\mathbf{W}^{(b)} \\ \mathbf{W}^{(b)\mathrm{T}}\mathbf{K}_{ba}^{e}\mathbf{W}^{(a)} & \mathbf{W}^{(b)\mathrm{T}}\mathbf{K}_{bb}^{e}\mathbf{W}^{(b)} \end{bmatrix} \begin{bmatrix} \mathbf{p}^{(a)} \\ \mathbf{p}^{(b)} \end{bmatrix} \tag{8}$$

2.2.3. Requirements for the waves

This section describes the physical meaning of the "waves", and presents requirements that must be met to be able to use the waves for wave-based substructuring. The waves can be seen as a special kind of modal displacement shapes that are defined at the substructure interface.

- Regarding the wave matrix size, recall from Section 2.2.1 that for each interface between substructures, the junction DOFs $\mathbf{x}_j^{(s)}$ of substructure (s) are expressed as a linear combination of a set of waves $\mathbf{W}^{(s)}$, weighted with wave participation factors $\mathbf{p}^{(s)}$. The dimension of $\mathbf{W}^{(s)}$ is hence $n_j^{(s)} \times n_w^{(s)}$, with $n_j^{(s)}$ the number of junction DOFs of the substructure and $n_w^{(s)}$ the number of wave vectors in $\mathbf{W}^{(s)}$. The wave matrix $\mathbf{W}^{(s)}$ hence has the same dimension as the matrix $\mathbf{\Phi}_j^{(s)}$, which is the partition of a modal displacement matrix $\mathbf{\Phi}^{(s)}$ with $n_w^{(s)}$ modes, defined at the $\mathbf{x}_j^{(s)}$ junction nodes of substructure (s).
- The waves and the modal displacement shapes (obtained from a modal analysis of the nominal full FE model of the complete structure) defined at the interface have a similar physical meaning.
  - In WBS, the waves are basis functions that must allow predicting the interface dynamics in a certain frequency range.
  - The modal displacement shapes at the interface are indeed a limited set of basis functions that one could use to describe the structural dynamics at the interface.

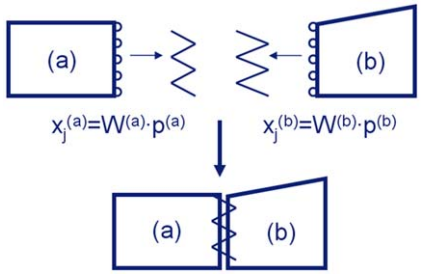

Fig. 2. Wave-based substructuring: example for the structure in Fig. 1, consisting of two substructures (a) and (b), with junction DOFs $\mathbf{x}_j^{(a)}$ and $\mathbf{x}_j^{(b)}$, and interior DOFs $\mathbf{x}_i^{(a)}$ and $\mathbf{x}_i^{(b)}$, respectively. The junction DOFs are expressed in terms of waves, and the assembly is defined between the wave participation factors.

- *Orthonormality* of the waves is recommended. It is key, for a given number of waves, to span a vector space as wide as possible. This is achieved with an orthonormal wave set. Furthermore, an orthonormal set is required to obtain a well-conditioned structural analysis problem after the wave substitution in Eq. (5), and hence to avoid poor quality of solutions or unstable solutions. In the limit case that a wave set contains duplicate individual waves, the numerical solver will yield a failure. In case of an elastic WBS connection, orthogonality of the waves is also required in order to avoid ill-conditioning of the elastic connection matrix defined in Eq. (8). Here it is noted that in a numerical implementation of an orthonormalization algorithm, perfect mathematical orthogonality of waves is typically not achieved. This is due to rounding and approximation errors in the lowest significant numbers in the wave definitions. In a practical wave calculation procedure, one must therefore perform a selection step to keep the most relevant waves that span the vector space of interest in order to accurately represent the interface deformations, while avoiding (slight) loss of conditioning. When one keeps waves that are of less importance to spanning the vector space of interest, one may introduce a limited ill-conditioning because of (minor) dependency effects with the other waves in the wave set.
- An additional requirement comes from the fact that the key value of WBS in the vehicle design process is seen in a modification and optimization context. To enable this, the wave set must be *robust to modifications*. That is, the set of waves $\mathbf{W}^{(s)}$ should not only enable to represent the interface dynamics of a nominal structure, but also the interface dynamics of a modified structure (e.g. the modification of one substructure, or the modification of elastic connection stiffness at the interface, in case of elastic WBS connection).

2.3. Procedure for wave-based substructuring

In the previous section, the WBS approach has been presented, and the matrix equations on a substructure level and assembly level have been introduced. Furthermore, it has been described that the waves can be regarded as a special kind of modal displacement shapes, defined at the junction DOFs of a substructure. Requirements for the waves have been described, both regarding the WBS matrix formulation and in view of practical applications. In this section, the WBS procedure for structural analysis is introduced. An outline of the procedure is shown in Fig. 3.

The wave calculation is described in detail in Section 2.3.1. First, a matrix of modal displacement shapes is obtained from a full FE analysis of the complete structure in the frequency range of interest. These modal displacement shapes are then postprocessed to obtain the waves (in order to guarantee orthogonality of individual waves and to perform a selection of waves). An option in the WBS procedure is to create a reduced modal model for components (i.e. substructures). The procedure for reduction of components is described in Section 2.3.2. The final step in the WBS procedure in Fig. 3 is the wave-based assembly definition between components, see Section 2.2.2.

2.3.1. Wave calculation

Consider a general undamped structure S decomposed into N_s substructures, to which no external forces are applied. For the nominal analysis case of interest, boundary conditions (in vehicle engineering, often free–free conditions) and a frequency range of interest have been specified. For this nominal structure S, a nominal full FE model is available, partitioned per substructure.

The aim of the wave calculation is to calculate a matrix $\mathbf{W}^{(s)}$ of $n_w^{(s)}$ waves for each substructure (s), so that the $n_j^{(s)}$ junction DOFs $\mathbf{x}_j^{(s)}$ can be written as linear combination of the waves according to Eq. (5). Provided that $n_w^{(s)} < n_j^{(s)}$, this reduces the size of the interface representation.

The first part of the wave calculation procedure consists of performing a modal analysis of the nominal full FE model of the complete structure S in the same frequency range as the nominal analysis case, and using the same boundary

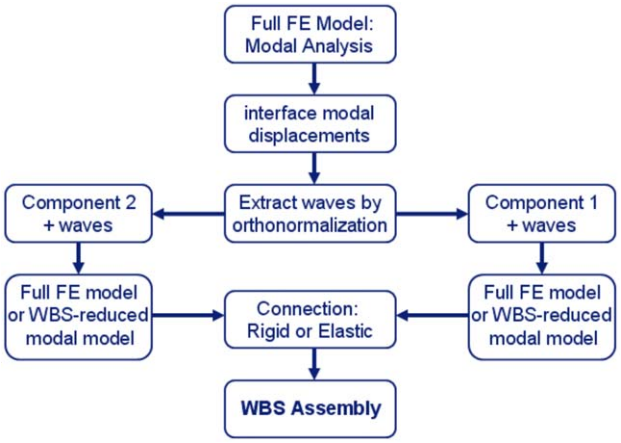

Fig. 3. Wave-based substructuring procedure.

conditions as the nominal model. This yields m eigenmodes $\mathbf{\Phi}$ (normal modes, optionally also residual attachment vectors), so that the displacement vector $\mathbf{x}$ can be written in approximate form as

$$\mathbf{x} \approx \hat{\mathbf{x}} = \sum_{m=1}^{N_r} \phi_r q_r = \mathbf{\Phi}\mathbf{q} \tag{9}$$

where the vector $\mathbf{q}$ contains the unknown eigenmode contribution factors q_r. This equation can then be partitioned per substructure, distinguishing interior DOFs $\mathbf{x}_i$ and junction DOFs $\mathbf{x}_j$:

$$\mathbf{x}_{N\times 1} = \mathbf{\Phi}_{N\times m}\mathbf{q}_{m\times 1} \iff \begin{bmatrix} \mathbf{x}_i^{(1)} \\ \mathbf{x}_j^{(1)} \\ \mathbf{x}_i^{(2)} \\ \mathbf{x}_j^{(2)} \\ \vdots \\ \mathbf{x}_i^{(s)} \\ \mathbf{x}_j^{(s)} \end{bmatrix} = \begin{bmatrix} \mathbf{\Phi}_i^{(1)} \\ \mathbf{\Phi}_j^{(1)} \\ \mathbf{\Phi}_i^{(2)} \\ \mathbf{\Phi}_j^{(2)} \\ \vdots \\ \mathbf{\Phi}_i^{(s)} \\ \mathbf{\Phi}_j^{(s)} \end{bmatrix} \cdot \{\mathbf{q}\} \tag{10}$$

The second part of the wave calculation aims at obtaining the wave sets $\mathbf{W}^{(s)}$ from the modal matrix $\mathbf{\Phi}$. For each interface, for each substructure (s), this second part starts from the matrix partition $\mathbf{\Phi}_j^{(s)}$ in Eq. (10) that contains the interface modal displacements obtained from the modal analysis of the nominal full FE model of the complete structure. Note that the individual vectors of $\mathbf{\Phi}_j^{(s)}$ do not (necessarily) meet the orthonormality requirement of the waves as introduced in Section 2.2.3:

- By performing the modal analysis calculation of the full FE model of the complete structure, a matrix of m eigenvectors $\mathbf{\Phi}$ is obtained; these eigenvectors are orthonormal in the subspace of the entire structure. For the individual vectors in the partition $\mathbf{\Phi}_j^{(s)}$ defined at the junction DOFs of one substructure, orthonormality is, however, not guaranteed. For instance, one can think of two modes that have very different modal displacement shapes in several regions of the structure (which makes them independent), but which have the same modal displacement shape at the particular interface of interest. In such case, the partitions of those two modes at the interface are linearly dependent.
- Postprocessing of $\mathbf{\Phi}_j^{(s)}$ must thus be performed, aimed at *orthonormalization* of the individual vectors of $\mathbf{\Phi}_j^{(s)}$. This moreover implies a *selection* of waves: when some of the vectors in $\mathbf{\Phi}_j^{(s)}$ are (approximately) linear combinations of the other vectors, they should be removed from the set. The postprocessing step aims at selecting the *minimum number of waves* that can represent the deformations at the substructure interface corresponding to the normal modes behavior of the full FE model of the complete structure.

The second part of the wave calculation can thus be summarized as partitioning the modal matrix $\mathbf{\Phi}$ to obtain the modal displacement vectors $\mathbf{\Phi}_j^{(s)}$ at the interface per substructure, and performing an orthonormalization and selection step to obtain waves with the characteristics required for WBS. Below, a practical procedure for this purpose is outlined. Calculating the waves $\mathbf{W}^{(s)}$ for a substructure (s) requires performing the following five steps:

(1) Create an $n_j^{(s)} \times m$ matrix $\mathbf{\Phi}_j^{(s)}$ that contains the interface modal displacements (see Eq. (10)), obtained from the modal analysis of the nominal full FE model of the complete structure.
(2) Normalize a priori each column vector in $\mathbf{\Phi}_j^{(s)}$ (i.e. each modal displacement shape at the interface) to unity:

$$\tilde{\mathbf{\Phi}}_j^{(s)} = \mathbf{\Phi}_j^{(s)} \cdot \operatorname{diag}\left(\frac{1}{\operatorname{diag}((\mathbf{\Phi}_j^{(s)})^{\mathrm{T}} \cdot \mathbf{\Phi}_j^{(s)})}\right) \tag{11}$$

(3) Perform an orthonormalization of the interface modal displacement matrix $\tilde{\mathbf{\Phi}}_j^{(s)}$. For this purpose the Singular Value Decomposition (SVD) as given in Eq. (12) is used:

$$\tilde{\mathbf{\Phi}}_j^{(s)} = \mathbf{U}_{n_j^{(s)}\times n_j^{(s)}} \mathbf{\Sigma}_{n_j^{(s)}\times m} \mathbf{V}^{\mathrm{T}}_{m\times m} \tag{12}$$

A visual representation of the SVD matrix equation is given in Fig. 4. The following characteristics are relevant for the WBS procedure:

- The SVD can be used for the orthonormalization when $m \leqslant n_j^{(s)}$. This is not a limitation for practical purposes. WBS is intended to be used for cases with a large interface DOF size; in that case, there will typically be (much) more interface DOFs $n_j^{(s)}$ than modes m in a frequency range of interest. (In case $m > n_j^{(s)}$, one may wish to reconsider the use of WBS, or one can choose for another orthonormalization algorithm, such as QR factorization [25].)
- The matrix $\mathbf{\Sigma}_m$ (the top $m \times m$ part of $\mathbf{\Sigma}$) contains the m singular values σ_i along the diagonal, in descending order (i.e. $\sigma_i \leqslant \sigma_{i-1}$ for all $i = 2..m$).
- The matrix $\mathbf{U}$ contains m orthonormal column vectors, which are the waves of interest.

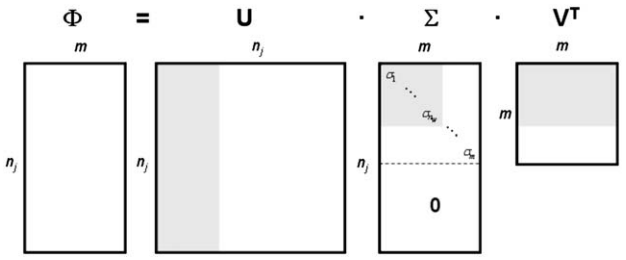

Fig. 4. SVD: visual representation of the SVD matrix equation in Eq. (12). For clarity, the substructure indices $^{(s)}$ are omitted. The selection procedure of the $n_w^{(s)}$ singular values has been visualized with the gray areas in the matrices.

(4) A selection of waves must then be made according to the matrix $\mathbf{\Sigma}_m$. The recommended practice is to apply a relative threshold T on the minimum value of the quantity σ_i/σ_1 that is allowed. For this purpose, the following procedure is applied to the singular value matrix $\mathbf{\Sigma}_m$:
- Normalize all singular values σ_i with the largest singular value σ_1.
- Subsequently apply a relative threshold T on the minimum value of the quantity σ_i/σ_1 that is allowed.
- Discard the singular values for which the quantity σ_i/σ_1 is smaller than the threshold T. That is: select all σ_i values for which

$$\sigma_i \geq T \cdot \sigma_1 \tag{13}$$

This leads to the selection of the first $n_w^{(s)}$ singular values.

(5) The wave matrix $\mathbf{W}^{(s)}$ is then obtained by selecting the first $n_w^{(s)}$ columns of the matrix $\mathbf{U}$.

In the visualized SVD matrix Eq. (12) in Fig. 4, the selection procedure is shown by means of the gray areas. The selection of $n_w^{(s)}$ singular values defines the gray square in the matrix $\mathbf{\Sigma}$; this leads to the selection of the wave matrix $\mathbf{W}^{(s)}$ as the first $n_w^{(s)}$ columns of the matrix $\mathbf{U}$, shown as the gray block area in matrix $\mathbf{U}$.

The condition number κ of the selected part of the matrix $\mathbf{\Sigma}$ (i.e. the gray square in Fig. 4) is given by $\sigma_1/\sigma_{n_w^{(s)}}$. This explains the recommended practice for wave selection in step 4: by applying a relative threshold T on the minimal quantity of σ_i/σ_1 that is allowed, one has direct control on the condition number of the selected part of $\mathbf{\Sigma}$, as one equivalently applies a threshold on the maximal condition number that is allowed. The larger the numerical condition number, the more ill-conditioned the WBS assembly system. Alternative methods to perform the singular value selection (e.g. applying an absolute threshold on the σ_i values, or selecting a fixed number of waves) do not provide such direct control on the condition number of the wave set.

Up to here, it has been explained how the wave matrices $\mathbf{W}^{(s)}$ for a substructure (s) can be calculated. The wave calculation procedure has been implemented as follows, in a modus operandi that depends on the type of connection:

Rigid connection: The waves $\mathbf{W}^{(a)}$ are calculated on one side of the connection using the procedure described above. These are then copied to the other side of the connection, so that $\mathbf{W}^{(a)} = \mathbf{W}^{(b)}$ by default. The rigid connection can then be made by applying Eq. (7).

Elastic connection: The waves $\mathbf{W}^{(a)}$ and $\mathbf{W}^{(b)}$ are calculated independently on each side of the connection. That is, using the above procedure, a separate SVD is performed on each side of the connection. This yields $n_w^{(a)}$ and $n_w^{(b)}$ waves, respectively, on each side ($n_w^{(a)}$ and $n_w^{(b)}$ may differ). The elastic connection can then be applied with Eq. (8).

2.3.2. Reduction of components

WBS can be applied directly between FE components, but fast assembly-level predictions can only be obtained when at least one of the components is reduced. In the WBS procedure, an efficient variant of the conventional reduction procedure of MacNeal and Rubin [16,17] can be used to reduce the components. Fig. 5 shows a conventional substructure, with interior DOFs $\mathbf{x}_i^{(s)}$ and junction DOFs $\mathbf{x}_j^{(s)}$. The conventional reduction procedure of MacNeal and Rubin [16,17] consists of calculating:

- the normal modes $\mathbf{\Phi}$ of the component in free–free conditions;
- the residual attachment modes $\mathbf{\Psi}_{ar}$ for each junction DOF. These are static deformation vectors that enable to accurately model the local flexibility at the interface. First, the residual stiffness matrix is calculated by subtracting the stiffness matrix of the normal component modes $\mathbf{\Phi}$ from the stiffness matrix in Eq. (2) (repeated below for clarity). This residual stiffness matrix then replaces the stiffness matrix in Eq. (2) in the static calculation procedure to obtain the residual

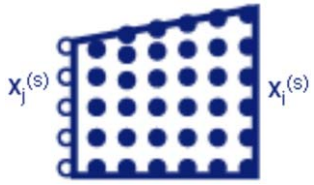

Fig. 5. Conventional substructure (s) with interior DOFs $\mathbf{x}_i^{(s)}$ and junction DOFs $\mathbf{x}_j^{(s)}$.

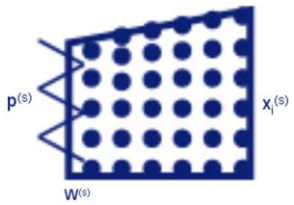

Fig. 6. WBS substructure (s) for WBS, with interior DOFs $\mathbf{x}_i^{(s)}$ and wave participation factors $\mathbf{p}^{(s)}$ at the junction.

attachment modes. A series of static analyses is performed, in which a unit force is applied at one junction DOF $\mathbf{x}_j$, with a zero force at the remaining junction DOFs; this procedure is repeated for all junction DOFs.

$$\begin{bmatrix} \mathbf{M}_{ii} & \mathbf{M}_{ij} \\ \mathbf{M}_{ji} & \mathbf{M}_{jj} \end{bmatrix}^{(s)} \begin{Bmatrix} \ddot{\mathbf{x}}_i \\ \ddot{\mathbf{x}}_j \end{Bmatrix}^{(s)} + \begin{bmatrix} \mathbf{K}_{ii} & \mathbf{K}_{ij} \\ \mathbf{K}_{ji} & \mathbf{K}_{jj} \end{bmatrix}^{(s)} \begin{Bmatrix} \mathbf{x}_i \\ \mathbf{x}_j \end{Bmatrix}^{(s)} = \begin{Bmatrix} 0 \\ \mathbf{f}_j \end{Bmatrix}^{(s)}$$

After this reduction calculation, the substructure can be reduced in terms of $\mathbf{\Phi}$ and $\mathbf{\Psi}_{ar}$ according to

$$\begin{Bmatrix} \mathbf{x}_i \\ \mathbf{x}_j \end{Bmatrix} = \begin{bmatrix} \mathbf{\Phi} & \mathbf{\Psi}_{ar} \end{bmatrix} \begin{Bmatrix} \mathbf{q} \\ \mathbf{r} \end{Bmatrix} = \begin{bmatrix} \mathbf{\Phi}_i & \mathbf{\Psi}_{ar,i} \\ \mathbf{\Phi}_j & \mathbf{\Psi}_{ar,j} \end{bmatrix} \begin{Bmatrix} \mathbf{q} \\ \mathbf{r} \end{Bmatrix} \tag{14}$$

Fig. 6 shows a substructure for WBS, with interior DOFs $\mathbf{x}_i^{(s)}$. The physical junction DOFs $\mathbf{x}_j^{(s)}$ are no longer used to represent the substructure interface: according to Eq. (5), the physical junction DOFs $\mathbf{x}_j^{(s)}$ have been expressed in terms of the waves $\mathbf{W}^{(s)}$, so that the wave participation factors $\mathbf{p}^{(s)}$ are now used to represent the substructure interface. Provided that $n_w^{(s)} < n_j^{(s)}$, this substitution reduces the size of the interface representation. In the latter case, the WBS approach results in a more efficient reduction procedure for substructures, which is elaborated below.

The equation of motion of a WBS substructure has been obtained in Section 2.2.1, by substituting Eq. (5) into Eq. (2). The resulting equation of motion has been presented in Eq. (6), which is repeated below for clarity:

$$\begin{bmatrix} \mathbf{M}_{ii} & \mathbf{M}_{ij}\mathbf{W} \\ \mathbf{W}^{\mathrm{T}}\mathbf{M}_{ji} & \mathbf{W}^{\mathrm{T}}\mathbf{M}_{jj}\mathbf{W} \end{bmatrix} \begin{Bmatrix} \ddot{\mathbf{x}}_i \\ \ddot{\mathbf{p}} \end{Bmatrix} + \begin{bmatrix} \mathbf{K}_{ii} & \mathbf{K}_{ij}\mathbf{W} \\ \mathbf{W}^{\mathrm{T}}\mathbf{K}_{ji} & \mathbf{W}^{\mathrm{T}}\mathbf{K}_{jj}\mathbf{W} \end{bmatrix} \begin{Bmatrix} \mathbf{x}_i \\ \mathbf{p} \end{Bmatrix} = \begin{Bmatrix} 0 \\ \mathbf{W}^{\mathrm{T}}\mathbf{f}_j \end{Bmatrix}$$

The WBS reduction procedure of the substructure system in Eq. (6) is now analogous to the conventional procedure of MacNeal and Rubin [16,17]. The WBS reduction procedure is as follows (the mode sets suffix $'$ indicates that they have been obtained in a WBS reduction procedure):

- calculate the normal modes $\mathbf{\Phi}'$ of the system in Eq. (6) in free–free conditions (note: this means free–free in terms of the interior DOFs $\mathbf{x}_i^{(s)}$ and the wave participation factors $\mathbf{p}^{(s)}$);
- calculate the residual attachment modes $\mathbf{\Psi}'_{ar}$ for each wave participation factor $\mathbf{p}^{(s)}$. First, the residual stiffness matrix is calculated by subtracting the stiffness matrix of the normal modes $\mathbf{\Phi}'$ from the stiffness matrix in Eq. (6). This residual stiffness matrix then replaces the stiffness matrix in Eq. (6) in the static calculation procedure to obtain the residual attachment modes. These static deformation shapes are obtained by successively applying a unit force $\mathbf{W}^{\mathrm{T}}\mathbf{f}_j$ (denoted "wave load vector") on one of the wave participation factors $\mathbf{p}$, with a zero force on the remaining wave participation factors, and repeating this for all wave participation factors. The unit force $\mathbf{f}_j$ is hence weighted with the wave shape of interest $\mathbf{W}^{\mathrm{T}}$ for each participation factor $\mathbf{p}$. Physically, this corresponds to applying a unit load to the entire interface (distributed according to the wave shape of interest). Provided that $\mathbf{p} < \mathbf{x}_j^b$, one thus obtains a smaller set of residual attachment modes that allow representing the local interface flexibility in assembly conditions.

After this WBS reduction calculation, the substructure can again be reduced in analogy with Eq. (14), in terms of the free–free component modes $\mathbf{\Phi}'$ and the (smaller set of) residual attachment modes $\mathbf{\Psi}'_{ar}$:

$$\begin{Bmatrix} \mathbf{x}_i \\ \mathbf{x}_j \end{Bmatrix} = \begin{bmatrix} \mathbf{\Phi}' & \mathbf{\Psi}'_{ar} \end{bmatrix} \begin{Bmatrix} \mathbf{q} \\ \mathbf{r} \end{Bmatrix} = \begin{bmatrix} \mathbf{\Phi}'_i & \mathbf{\Psi}'_{ar,i} \\ \mathbf{\Phi}'_j & \mathbf{\Psi}'_{ar,j} \end{bmatrix} \begin{Bmatrix} \mathbf{q} \\ \mathbf{r} \end{Bmatrix} \tag{15}$$

As mentioned, the WBS substructure system equation in Eq. (6) is free–free in the sense that the interior DOFs $\mathbf{x}_i$ and the wave participation factors $\mathbf{p}$ are free in the substructure solution procedure. However, by substituting Eq. (5) in Eq. (2), assembly-level dynamic boundary conditions have been introduced. The original junction DOFs $\mathbf{x}_j^b$ have been expressed in terms of the waves $\mathbf{W}^{(s)}$ using Eq. (6). Recall that the waves $\mathbf{W}^{(s)}$ have been obtained by orthonormalizing the interface modal displacement matrix $\mathbf{\Phi}_j^{(s)}$, which comes from a full FE modal analysis of the assembled nominal model. Physically, this brings already some assembly-level behavior into the substructure behavior. The interface can only behave as linear combination of the waves $\mathbf{W}^{(s)}$, weighted with the wave participation factors $\mathbf{p}$. As a bonus (added to the more efficient reduction procedure), this may also improve the quality of the substructure modal basis for assembly-level predictions.

3. Validation cases

In this section, WBS is applied to two cases, namely a two-plate assembly case and an industrial vehicle BIW case. To assess the efficiency and accuracy of WBS, comparisons are made with the full FE analysis and the conventional MacNeal–Rubin substructuring procedure. For all the calculations, MSC.Nastran [26] has been used as FE solver, MATLAB [27] has been used for file pre- and postprocessing and intermediate calculations, and LMS Virtual.Lab [28] has been used to assess the correlation between mode sets with the modal assurance criterion (MAC) [29].

3.1. Two-plate assembly

3.1.1. Case description

Fig. 7 shows a two-plate assembly made of steel (Young's modulus $E = 210$ GPa, Poisson coefficient $\nu = 0.3$, mass density $\rho = 7850\,\mathrm{kg/m^3}$). In terms of geometry, Plate A and Plate B have the following dimensions:

- Plate A measures 0.5 m by 0.5 m in a wedge shape, with a thickness of 1 mm. It consists of 441 nodes and 400 quad elements.
- Plate B (434 nodes, 789 tria elements) measures 0.434 m by 0.3 m has a thickness of 0.85 mm and makes an angle of 31° with the Plate A plane.
- The interface is defined between 21 coincident nodes on each side, i.e. there are 126 junction DOFs. A rigid connection is applied.

Plate A is larger and slightly thicker than Plate B. Free–free component modal analysis of Plate A resp. Plate B yields 20 resp. 16 normal modes (incl. 6 rigid body modes) up to 150 Hz. In this section, all FE calculations have been performed on an Intel Pentium4 2813 computer system (1 GHz, 2 GB RAM) running a Windows 2000 operating system, using MSC.Nastran version 2001.0.1.

3.1.2. Results

To verify WBS, an assembly is created of a full FE Plate A and a WBS-reduced modal model of Plate B, valid in the range $[0, 100]$ Hz:

- A full FE modal analysis is performed in the range [0,100] Hz (CPU time 12.3 s); there are 22 modes (incl. 6 rigid body modes).
- An orthonormalization is performed using the SVD in Eq. (12), without setting an SVD threshold T as in Eq. (13), so that all 22 waves are kept. These 22 wave DOFs are used for an efficient representation of the interface (instead of the 126 junction DOFs).

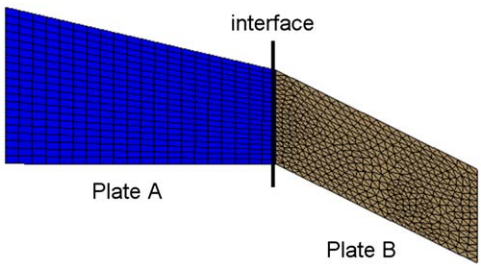

Fig. 7. Wave-based substructuring: two-plate assembly structure.

- Plate B is reduced using the procedure described in Section 2.3.2. The substructure solution consists of calculating the substructure modes up to 150 Hz, and the residual attachment modes for the 22 wave participation factors.
- A rigid connection between the wave participation factors is created, yielding the WBS assembly structure.

Table 1 and Fig. 8 show the WBS process characteristics and the accuracy of WBS results. Among others, it can be seen that the relative eigenfrequency difference is less than 7.7×10^{-5}, and the minimal MAC diagonal is 0.999973, when compared to the full FE results.

Table 1 and Fig. 8 also show the results of the conventional procedure according to MacNeal and Rubin [16,17]. Again, an assembly of Plate A (full FE) and Plate B (reduced) is made for the range $[0, 100]$ Hz:

- Plate B is reduced according to MacNeal: a free–free modal analysis up to 150 Hz, asking residual attachment modes for all 126 junction DOFs; thereof, only 102 are provided by MSC.Nastran. Due to approximation errors in the numerical implementation, not all individual residual attachment modes can be distinguished, as their shapes are quite similar. The solver then does not provide the entire basis of residual attachment modes, one for each physical junction DOF.
- The MacNeal assembly structure is created through rigid connections between the physical junction DOFs.

The results in Table 1 indicate that WBS offers a benefit for the reduction phase and the assembly phase:

- The reduction time and reduced modal model size for Plate B are smaller, as less residual attachment modes are required.
- The assembly solution time is slightly smaller, since the WBS model has a smaller interface representation size between the components, and involves coupling a smaller-sized reduced modal model for Plate B.

From a methodological perspective, it can be expected that WBS assembly prediction results are more accurate than the results with MacNeal. The reason is that in WBS, assembly-level waves $\mathbf{W}^{(s)}$ are used to describe the interface behavior on the substructure level. This brings already some assembly-level behavior into the substructure behavior, which improves

Table 1
Two-plate assembly structure (see Fig. 7): Plate A full FE, Plate B in reduced modal model, using MacNeal or WBS, compared to full FE results.

	MacNeal	WBS
Number of component normal modes	16	16
Number of residual attachment modes	102 (out of 126)	22
CPU time reduction	12.3 s	6.5 s
Reduced model size	1902 kb	400 kb
CPU time assembly	6.6 s	6.4 s
Rel. eigfreq. diff: average	5.0×10^{-5}	1.2×10^{-5}
Rel. eigfreq. diff: maximum	3.9×10^{-4}	7.7×10^{-5}
MAC diagonal: average	0.999983	0.999996
MAC diagonal: minimum	0.999813	0.999973

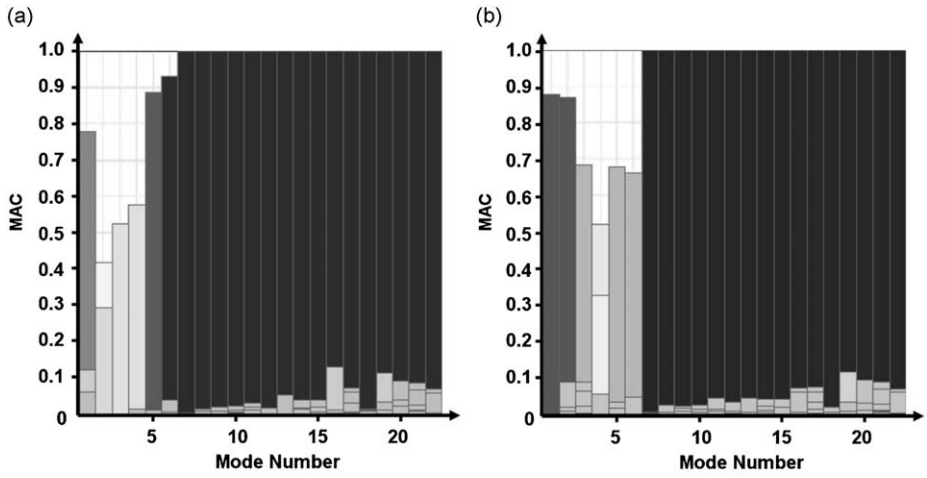

Fig. 8. Two-plate assembly structure (see Fig. 7). An assembly (full FE Plate A, and reduced Plate B) has been created, using (a) MacNeal and (b) WBS for the reduction. The MAC (w.r.t. full FE results) is shown for both cases.

the quality of the modal reduction basis. However, the method comparison in Table 1 and Fig. 8 is not conclusive in terms of accuracy, given the very small absolute prediction errors with both WBS and MacNeal, and given the very small differences in the results for both methods.

3.2. Industrial vehicle model: B-pillar case

3.2.1. Case description

Fig. 9(a) shows an industrial vehicle BIW model (230.183 nodes, 223.323 elements) made of steel (Young's modulus $E = 210$ GPa, Poisson coefficient $\nu = 0.3$, mass density $\rho = 7890\,\mathrm{kg/m^3}$). The BIW consists of two rigidly connected substructures:

- The B-pillars (14.699 nodes and 13.697 elements), see Fig. 9(b).
- The body remainder (215.484 nodes and 209.328 elements), see Fig. 9(c).
- The connection consists of 298 junction nodes (i.e. 1788 junction DOFs).

In this section, WBS is applied in the B-pillar design scenario. The reduced modal model of interest has the B-pillars in FE representation and a reduced modal model for the vehicle BIW remainder, as shown in Fig. 9(d). For this scenario, the performance and prediction accuracy are compared to classical substructuring according to MacNeal and Rubin [16,17]. It will be shown that WBS is much more efficient than conventional substructuring, and hence enables efficient B-pillar design modification. All calculations have been performed on an Intel Xeon 5150 computer system (2.66 GHz, 8 GB RAM, with 750 GB scratch space) running a Windows XP2003 SP2 x64 operating system, using MSC.Nastran version 2005.5.2.

3.2.2. Results

First, the procedure in Section 2.3 is applied to create a WBS assembly of the full FE B-pillars and a WBS-reduced modal model of the body remainder (see Fig. 9(d)), which is valid in the range $[0, 100]$ Hz:

- A full FE modal analysis is performed in the range $[0, 100]$ Hz (CPU time 26 m 28 s); there are 35 modes (incl. 6 rigid body modes).

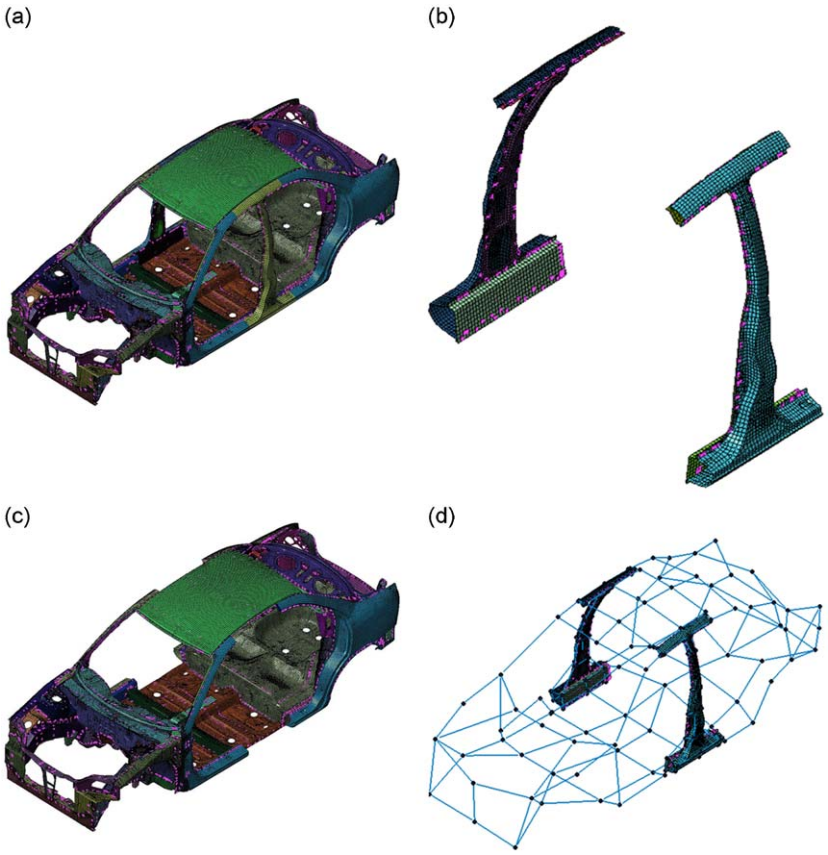

Fig. 9. Vehicle B-pillar case: industrial vehicle BIW FE model (a), which consists of two components: the B-pillars component (b) and the body remainder component (c). The reduced modal model of interest (d) has the B-pillars in FE representation and a reduced modal model for the vehicle BIW remainder.

- An SVD orthonormalization with threshold $T = 1 \times 10^{-6}$ in Eq. (13) is performed; all 35 waves are kept. In [30], it has been derived that an SVD threshold $T = 1 \times 10^{-6}$ is a suitable choice for engineering applications. After the waves selection, the 35 wave participation factors are used for an efficient interface representation (substituting 1788 junction DOFs).
- The BIW remainder is reduced using the procedure described in Section 2.3.2, by calculating the substructure modes up to 150 Hz and residual attachment modes only for the 35 wave participation factors.
- A rigid WBS connection is defined to create the WBS assembly.

Subsequently, also the conventional substructuring approach of MacNeal and Rubin [16,17] has been used to create a reduced assembly model as in Fig. 9(d). Again, an assembly of the B-pillars (full FE) and the BIW remainder (reduced) is made for the range $[0, 100]$ Hz:

- The BIW remainder is reduced with a conventional reduction, by calculating the substructure free–free natural modes up to 150 Hz, and asking residual attachment modes for all 1788 junction DOFs, of which only 1128 have been provided by the MSC.Nastran solver. Again, approximation errors in the numerical implementation have the result that it is not possible to distinguish all individual residual attachment modes, as their shapes are quite similar. Because of this, the solver does not provide the complete set of residual attachment modes, one for each physical junction DOF.
- The MacNeal assembly structure is created by defining rigid connections between the physical junction DOFs.

Table 2 shows the WBS process characteristics and the accuracy of results when compared to full FE: a relative eigenfrequency difference $< 4.7 \times 10^{-5}$ for each mode, and a minimal MAC diagonal value of 0.999847. Table 2 also shows the results of the conventional procedure [16,17].

When comparing the WBS and MacNeal results for the industrial BIW case, the tentative conclusions based on the two-plate assembly (see Table 1) are strongly confirmed for this industrial case. In fact, the benefits of WBS in terms of accuracy and efficiency are much more apparent:

- The reduction time for WBS (< 1 h) is much smaller than for MacNeal (> 26 h); also the reduced model size with WBS (less than 4 MB) is much smaller than with MacNeal (193 MB).
- The WBS assembly predictions are significantly faster (41.7 s, where MacNeal requires 181 s), and much more accurate. With WBS, the relative eigenfrequency difference is three orders of magnitude smaller and the maximal MAC deviation from 1 is only 1.53×10^{-4}. With MacNeal, Fig. 10 shows that the MAC Minimum can be as low as 0.23, so that the MAC deviation from unity attains values up to 0.77.

For this case, the MacNeal reduction procedure is clearly inefficient, and does not result in a suitable component modal basis for accurate assembly predictions. The relative eigenfrequency error up to $+5$ percent (i.e. a stiffening effect) is due to locking [18]: the incomplete set of 1128 residual attachment modes is insufficient to accurately represent the local flexibility at the interface.

In summary, WBS offers a clear efficiency and accuracy benefit over the conventional MacNeal reduction procedure, especially for cases with large interface size between substructures, as WBS allows modeling the local flexibility at the interface with just a few enrichment vectors. It also brings some assembly-level behavior into the substructure behavior. The combined effect results in a smaller and more accurate basis of substructure modes.

4. Robust modification predictions with WBS

In this section, it is shown that wave-based substructuring can be used for efficient modification analysis, which is key towards vibro-acoustic optimization and robust design. The vehicle B-pillar case as shown in Fig. 9 is revisited. The effect of B-pillar modifications on the global vehicle dynamics is assessed, based on the WBS-reduced assembly model in Fig. 9(d). It

Table 2
Vehicle B-pillar case (see Fig. 9): B-pillars are kept in FE representation, and a reduced modal model is created for the remainder of the vehicle BIW, using MacNeal or WBS, compared to full FE results.

	MacNeal	WBS
Number of component normal modes	85	70
Number of residual attachment modes	1128 (out of 1788)	35
CPU time reduction	26 h 40 min 29 s	54 min 13 s
Reduced model size	193 MB	3.94 MB
CPU time assembly	181 s	41.7 s
Rel. eigfreq. diff: average	1.9×10^{-2}	1.3×10^{-5}
Rel. eigfreq. diff: maximum	4.9×10^{-2}	4.7×10^{-5}
MAC diagonal: average	0.87810	0.999986
MAC diagonal: minimum	0.22906	0.999847

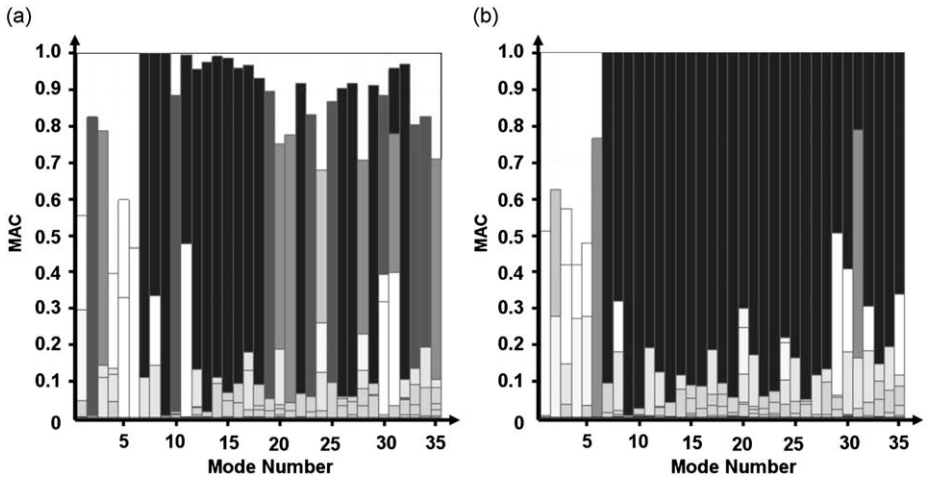

Fig. 10. Vehicle B-pillar case (see Fig. 9): an assembly (B-pillars in FE representation, and a reduced modal model for the remainder of the vehicle BIW) has been created, using (a) MacNeal or (b) WBS for the reduction (see Table 2). The MAC (w.r.t. full FE results) is shown in side view for both cases.

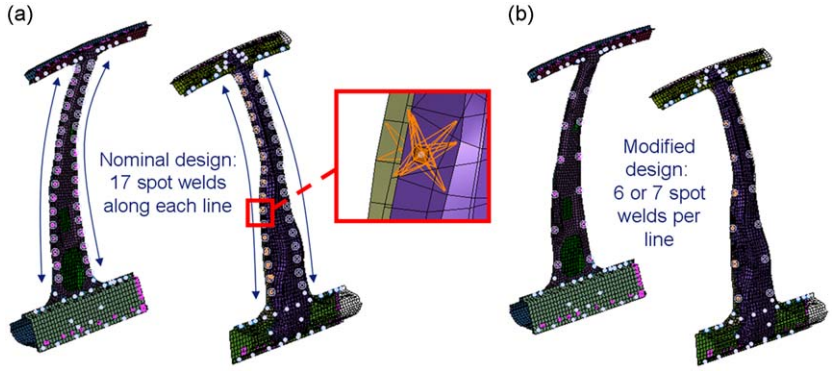

Fig. 11. Vehicle B-pillar case: modification of spot weld layout from the nominal design (a) to a modified design with a sparse spot weld density (b).

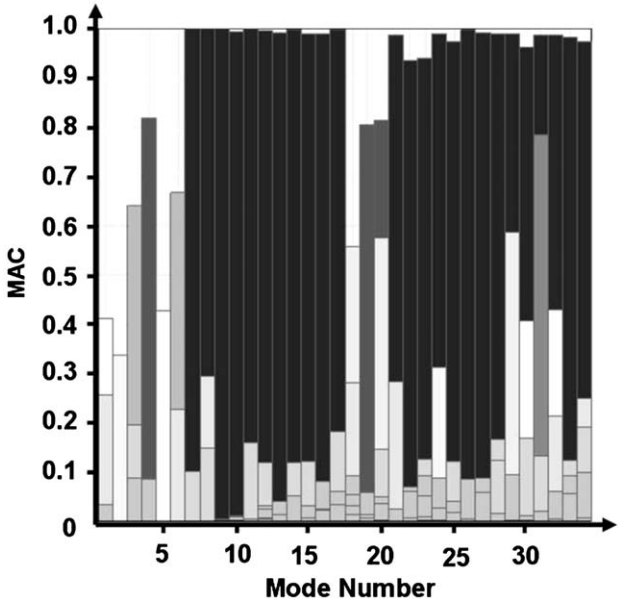

Fig. 12. Vehicle B-pillar spot weld layout modification: MAC to compare the nominal modes (with B-pillars as in Fig. 11(a)) with the modes obtained when the B-pillars are modified (Fig. 11(b)).

has been shown in Section 3.2 that the use of 35 waves instead of 1788 physical DOFs improves the efficiency of the reduction procedure and the accuracy of assembly predictions when compared to a conventional MacNeal–Rubin reduction. The substructuring in Fig. 9(d) is aimed at efficient design modification of the B-pillar and its joint connections to the body. Two cases are presented: spot weld layout modification, and local reinforcement of the B-pillar and the B-pillar to rocker joint.

4.1. Spot weld layout modification

The nominal B-pillars have been spot welded along four line connections with an average spot weld distance of 55 mm, so that 17 spot welds are created along each line, see Fig. 11(a). In the modified design, the distance is increased to 150 mm, so that the number of spot welds along each line is drastically reduced to only 6 or 7 per connection line, see Fig. 11(b).

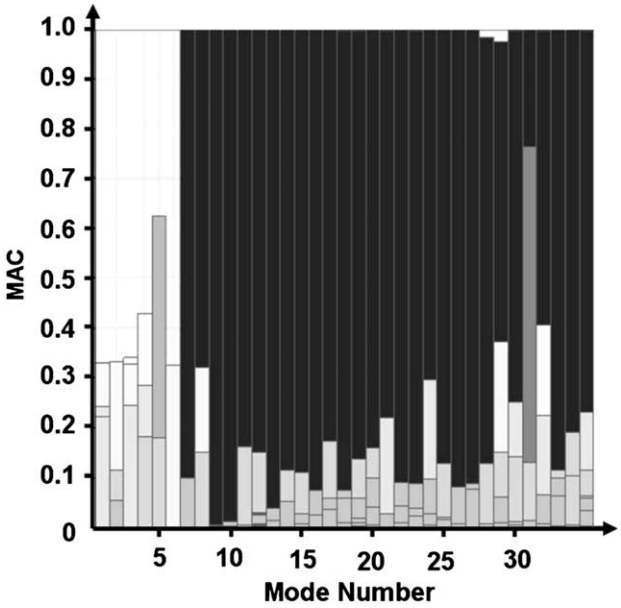

Fig. 13. Vehicle B-pillar spot weld layout modification: MAC to compare the modes obtained with the modified B-pillars (Fig. 11(b)) in the WBS reduced assembly case with those of a full FE validation analysis.

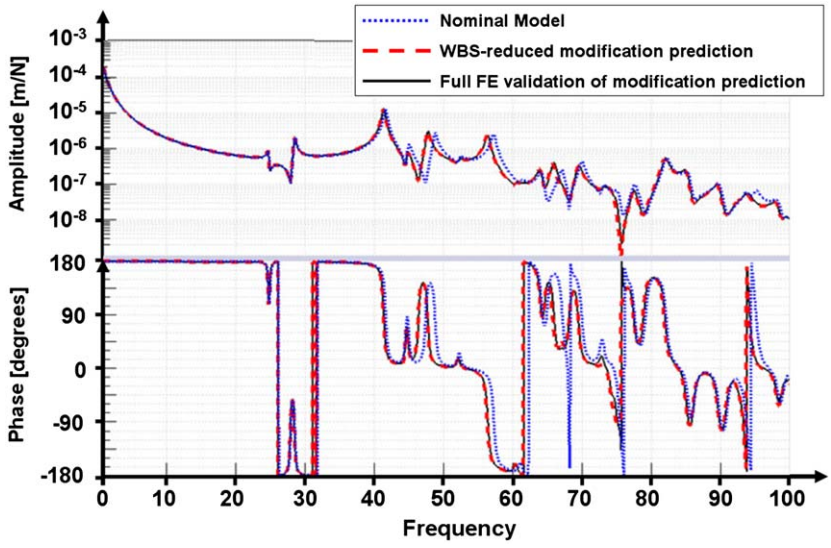

Fig. 14. Vehicle B-pillar spot weld layout modification: FRF from engine mount ($+Z$) to seat rail ($+Z$) ([0−100] Hz). The nominal model (17 spot welds per line) yields the dotted curve. For the modified models (6 or 7 spot welds per line), the WBS-reduced result (solid) is compared with the full FE validation result (dashed).

For this modification, Fig. 12 compares the full FE analysis results for the nominal model and the model with the B-pillars modified as in Fig. 11(b), i.e. with 6 or 7 spot welds instead of 17 spot welds along each line. The dynamics have clearly changed as a result of the modification.

To assess the quality of the modification prediction with WBS, a comparison is made between the modes of the BIW with modified B-pillars, see Fig. 11(b), obtained from a full FE validation analysis of the modified model, and from a WBS-reduced assembly analysis. For all modes up to 100 Hz, the relative eigenfrequency difference is less than 0.3 percent, and the MAC diagonal value is larger than 0.98 (see Fig. 13).

Finally, Fig. 14 shows the results of a structural FRF calculation. More specifically, the displacement over force FRF is calculated in the range up to 100 Hz, with input force at the engine mount ($+z$) and output at the driver seat rail ($+z$). The nominal FRF, shown as a dotted line, is compared with the FRFs obtained from the modified models (with 6 or 7 spot welds along each line). The modification prediction with the WBS-reduced assembly model (solid) is compared with a full FE validation analysis (dashed). It can be seen that the effects of the modification are noticeable (the nominal curve clearly differs from the modified curves), and that the WBS-reduced modification prediction is very accurate when compared to the full FE validation prediction of the modification, both in terms of amplitude and phase.

4.2. Local reinforcement of the B-pillar

In this section, local reinforcements are applied to the B-pillar, which are efficiently evaluated using the WBS-reduced modal model of Section 3.2.

- At each side, a flange with 2 mm thickness has been applied at the top of the B-pillar (see Fig. 15, top), located between the central panel and the outer shell, and connected with two additional spot welds.
- At each side, two reinforcement panels have been added inside the B-pillar to rocker joint (see Fig. 15, bottom), with a shell thickness of 1.5 mm. They are connected inside the rocker joint with seam welds.

Such local modifications are often applied in a vehicle (re)design context, for instance when creating variants for different markets (e.g. in case of different body stiffness requirements or side impact regulations in these markets). For this modification, Fig. 16 compares the full FE analysis results for the nominal model and the modified model in which the local reinforcements shown in Fig. 15 have been added. The dynamics have clearly changed as a result of the modification.

To assess the quality of the modification prediction with WBS, a comparison is made between the modes of the BIW with modified B-pillars (as in Fig. 15), obtained from a full FE validation analysis of the modified model, and from a WBS-reduced assembly analysis. The relative eigenfrequency difference is less than 1.0 percent for all modes up to 100 Hz, and the MAC diagonal value is larger than 0.97 for all modes up to 100 Hz, see also Fig. 17.

The cases presented in this section show that WBS can be applied for efficient design modification, which is key in view of optimization and robust design. In this section, efficient design modification of the B-pillar and its joint connections to the vehicle body have been considered. The WBS-reduced modal model has been used (see Fig. 9(d)), with the B-pillars in FE representation and a reduced modal model for the vehicle BIW remainder. The B-pillars have a large interface size

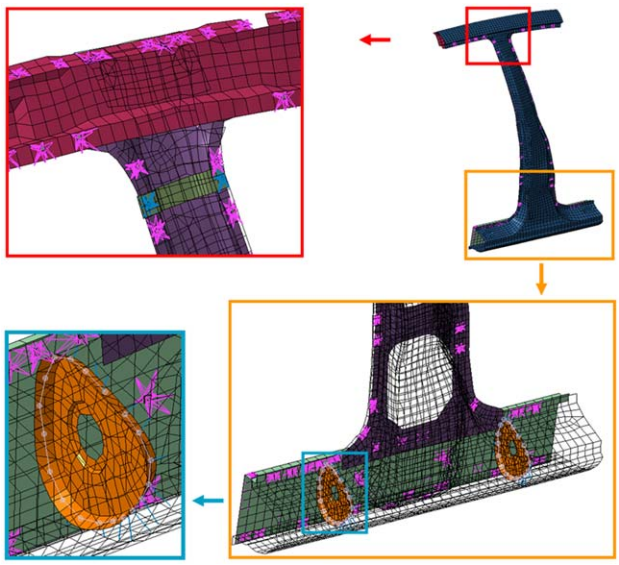

Fig. 15. Vehicle B-pillar case: local reinforcements are added to the B-pillar and the B-pillar to rocker joint.

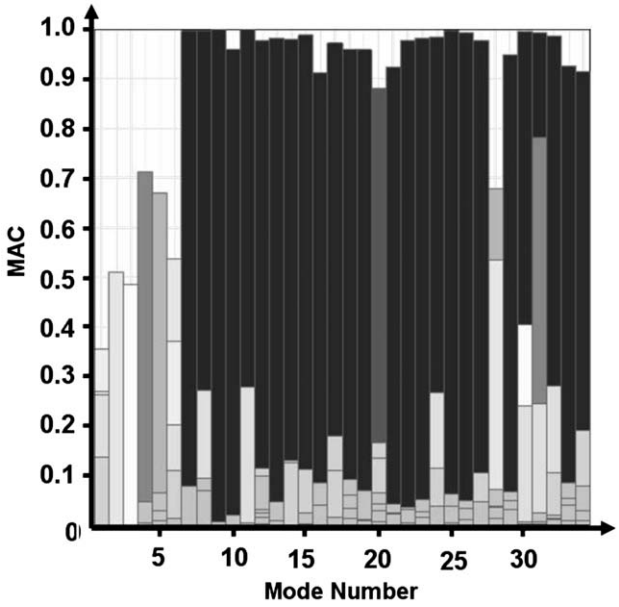

Fig. 16. Vehicle B-pillar local reinforcement: MAC to compare the modes of the nominal model with the modes obtained when local reinforcements are added (see Fig. 15).

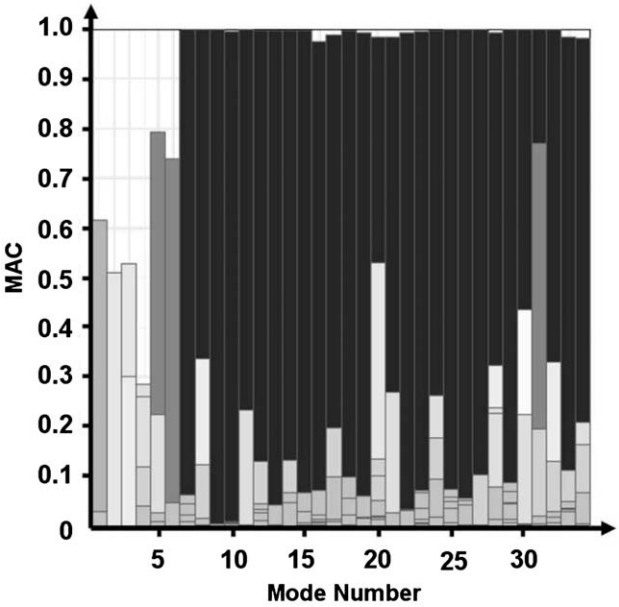

Fig. 17. Vehicle B-pillar local reinforcement: MAC to compare the modes for the modified structure using WBS and a full FE modification validation analysis.

(in terms of physical DOFs) to the remainder of the BIW, so that classical substructuring according to MacNeal and Rubin is inefficient and even inaccurate. WBS, however, allows to make the required partitioning for efficient design modification of the B-pillar and its joints. Two structural modification scenarios have been shown: the modification of spot weld layout and the placement of local reinforcements. The modifications have a substantial effect on the global body modes, which is accurately predicted using the WBS-reduced modal model.

5. Conclusions

A wave-based substructuring (WBS) approach has been presented, which allows reducing the interface representation between substructures in an assembled system, by expressing the degrees of freedom at the interface in terms of a limited

set of basis functions (“waves”). Especially for structures with a large interface representation size in terms of physical DOFs, this provides a number of benefits as compared to the conventional procedure of MacNeal and Rubin:

- WBS improves the efficiency of the reduction procedure, since a lower number of residual attachment modes needs to be calculated;
- WBS may improve the accuracy of the reduction procedure. On the one hand, a conventional reduction procedure may result in inaccurate results: due to approximation errors in the numerical implementation, the solver may not be able to distinguish between all individual residual attachment modes, hence the calculation may only yield a subset. On the other hand, WBS uses globally defined waves in the reduction procedure of components to describe the interface behavior; this effectively constrains the interface to global behavior on component level, which results in a more accurate component modal basis for assembly-level predictions.
- WBS improves the efficiency of modification predictions using the WBS-reduced modal model. The interface representation size is reduced, and also the size of the reduced modal models of components is reduced (since the component reduction calculation involves the calculation of a lower number of residual attachment modes).
- WBS improves the prediction accuracy with the reduced assembly model (thanks to a more accurate component reduction procedure).

The efficiency and accuracy of WBS (as compared to the conventional MacNeal–Rubin substructuring procedure) have been demonstrated on the basis of two application cases, namely a two-plate assembly case and an industrial vehicle BIW case aimed at efficient re-design of the B-pillars. On the basis of the latter case, it has been shown that WBS can be used for efficient design modifications in view of reaching structural or vibro-acoustic performance targets. Especially in case of large interface size between the substructures, a common situation in vehicle industry (B-pillars, cowl top, roof or floor, etc.), WBS offers a clear benefit for vehicle design modifications, by drastically improving the speed of component reduction processes and by improving the efficiency and accuracy of design iteration predictions when compared to conventional substructuring approaches.

Acknowledgments

We kindly acknowledge IWT Vlaanderen for their support of the Project IWT-070337 “MIDAS—next generation numerical tools for mid-frequency acoustics”, and we gratefully acknowledge the European Commission for their support of the Collaborative Project CP-218508 “MID-MOD—Mid-frequency vibro-acoustic modelling tools”. Furthermore, Bert Pluymers wishes to acknowledge the Industrial Research Fund K.U.Leuven. Finally, we kindly acknowledge the European Commission for their support of the Marie Curie EST Project “SIMVIA2” (http://www.simvia2.eu, contract nr. MEST-CT-2005-020263), from which Mr. Patrik Ragnarsson holds a Research Training grant.

References

[1] G. Wöhlke, E. Schiller, Digital planning validation in automotive industry, *Computers in Industry* 56 (4) (2005) 393–405.
[2] M.S. Shephard, M.W. Beall, R.M. O'Bara, B.E. Webster, Toward simulation-based design, *Finite Elements in Analysis and Design* 40 (12) (2004) 1575–1598.
[3] M. Turner, R. Clough, H. Martin, L. Topp, Stiffness and deflection analysis of complex structures, *Journal of Aerospace Science* 23 (9) (1956) 805–823.
[4] O.C. Zienkiewicz, R.L. Taylor, J.Z. Zhu, P. Nithiarasu, *Finite Element Method—The Three Volume Set*, sixth ed., Butterworth-Heinemann, Boston, 2005.
[5] R. Freymann, *Advanced Numerical and Experimental Methods in the Field of Vehicle Structural-Acoustics*, Hieronymus Buchreproduktions GmbH, Munich, Germany, 2000.
[6] N.H. Kim, J. Dong, K.K. Choi, N. Vlahopoulos, Z.-D. Ma, M.P. Castanier, C. Pierre, Design sensitivity analysis for sequential structural-acoustic problems, *Journal of Sound and Vibration* 263 (3) (2003) 569–591.
[7] W. Desmet, B. Pluymers, P. Sas, Vibro-acoustic analysis procedures for the evaluation of the sound insulation characteristics of agricultural machinery cabins, *Journal of Sound and Vibration* 266 (2003) 407–441.
[8] P.J. Shorter, R.S. Langley, Vibro-acoustic analysis of complex systems, *Journal of Sound and Vibration* 288 (3) (2005) 669–699.
[9] B. Pluymers, B. Van Hal, D. Vandepitte, W. Desmet, Trefftz-based methods for time-harmonic acoustics, *Archives of Computational Methods in Engineering* 14 343–381.
[10] R.R. Craig Jr., *Structural Dynamics—An Introduction to Computer Methods*, Wiley, New York, 1981.
[11] D.-M. Tran, Component mode synthesis methods using interface modes. Application to structures with cyclic symmetry, *Computers & Structures* 79 (2) (2001) 209–222.
[12] M.A. Tournour, N. Atalla, O. Chiello, F. Sgard, Component mode synthesis methods using interface modes. Application to structures with cyclic symmetry, *Computers & Structures* 79 (2) (2001) 1861–1876.
[13] H. De Gersem, D. Moens, W. Desmet, D. Vandepitte, Interval and fuzzy dynamic analysis of finite element models with superelements, *Computers & Structures* 85 (2007) 304–319.
[14] L. Hinke, F. Dohnal, B.R. Mace, T.P. Waters, N.S. Ferguson, Component mode synthesis as a framework for uncertainty analysis, *Journal of Sound and Vibration* 324 (1–2) (2009) 161–178.
[15] R.R. Craig Jr., M.C.C. Bampton, Coupling of substructures for dynamic analyses, *AIAA Journal* 6 (7) (1968) 1313–1319.
[16] R.H. MacNeal, A hybrid method of component mode synthesis, *Computers & Structures* 1 (4) (1971) 581–601.
[17] S. Rubin, Improved component-mode representation for structural dynamic analysis, *AIAA Journal* 13 (8) (1975) 995–1006.
[18] E. Balmès, Use of generalized interface degrees of freedom in component mode synthesis, *Proceedings of IMAC XIV*, Dearborn, MI, USA, 1996, pp. 204–210.

[19] L. Ji, B. Mace, R.J. Pinnington, A hybrid mode Fourier-transform approach for estimating the vibrations of beam-stiffened plate systems, *Journal of Sound and Vibration* 274 (3–5) (2004) 547–565.
[20] K. Brahmi, N. Bouhaddi, R. Fillod, Reduction of junction degrees of freedom in certain methods of dynamic substructure synthesis, *Proceedings of IMAC XIII*, Nashville, TN, USA, 1995, pp. 1763–1769.
[21] M.P. Castanier, Y.-C. Tan, C. Pierre, Characteristic constraint modes for component mode synthesis, *AIAA Journal* 39 (6) (2001) 1182–1187.
[22] G. Masson, B. Ait Brik, S. Cogan, N. Bouhaddi, Component mode synthesis (CMS) based on an enriched Ritz approach for efficient structural optimization, *Journal of Sound and Vibration* 296 (4–5) (2006) 845–860.
[23] S. Donders, R. Hadjit, K. Cuppens, M. Brughmans, W. Desmet, A wave-based substructuring approach for faster vehicle assembly predictions, *Proceedings of NOVEM 2005*, Saint-Raphaël, France, April 18–21, 2005.
[24] S. Donders, R. Hadjit, M. Brughmans, L. Hermans, W. Desmet, A wave-based substructuring approach for fast modification predictions and industrial vehicle optimization, *Proceedings of ISMA 2006*, Leuven, Belgium, September 18–20, 2006, pp. 1901–1912.
[25] Y. Saad, *Iterative Methods for Sparse Linear Systems*, second ed., SIAM, Philadelphia, PA, 2000.
[26] MSC. MSC/Nastran 2004, 2004.
[27] The MathWorks Inc. MATLAB Version 6.5, June 2002.
[28] LMS International. LMS Virtual.Lab Rev 6B, November 2006.
[29] W. Heylen, S. Lammens, P. Sas, *Modal Analysis Theory and Testing*, second ed., Katholieke Universiteit Leuven, Department of Mechanical Engineering, 1997.
[30] S. Donders, Computer-aided Engineering Methodologies for Robust Automotive NVH Design, PhD Thesis, K.U.Leuven, Department of Mechanical Engineering, Division PMA, Leuven, Belgium, February 2008.